RSC Advances

ROYAL SOCIETY OF CHEMISTRY

www.rsc.org/advances

Uniaxial pressure induced phase transitions in multiferroic materials $BiCoO_3$

Xing Ming,[1,2] Xing Meng,[2] Qiao-Ling Xu,[2] Fei Du,[2] Ying-Jin Wei,[2] and Gang Chen[2,3*]

1 College of Physics and Electronic Information, Huanggang Normal University, Huanggang 438000, P. R. China

2 Key Laboratory of Physics and Technology for Advanced Batteries (Ministry of Education) and College of Physics, Jilin University, Changchun 130012, P. R. China

3 State Key Laboratory of Superhard Materials and College of Physics, Jilin University, Changchun 130012, P. R. China

*Corresponding author.

E-mail: mingxing06@mails.jlu.edu.cn

ABSTRACT

The crystallographic structure stability, spin state and electronic structure variation in tetragonal multiferroic material $BiCoO_3$ under uniaxial pressure are investigated by means of first-principles density functional theory calculations. The lattice parameters, atomic internal coordinate and magnetic moment change abruptly under *c* axis compression of 9 GPa. A first-order structural phase transition occurs with a unit cell volume collapse of 9.5%, accompanying by the Co-O coordination polyhedron changing from CoO_5 pyramid to the distorted CoO_6 octahedron. A spin state transition of the Co^{3+} ions from the high-spin configuration in the CoO_5 pyramidal coordination to the nonmagnetic low-spin configurations in the distorted CoO_6 octahedron coordination has been explored. Contrasted electronic structure calculations are performed with PBE Generalized Gradient Approximation (GGA) and B3LYP hybrid functional. The hybrid functional drastically improves the band gap of the ground state. A controversial electronic structure has been predicted by GGA-PBE and B3LYP hybrid functional for the high pressure phase $BiCoO_3$. We propose that the high pressure phase $BiCoO_3$ is a nonmagnetic insulator.

I. INTRODUCTION

The parallel technological achievements both in magnetic materials and ferroelectric materials have attracted great interest in magnetoelectric materials, in which magnetic and electric polarization are strongly coupled.[1] Magnetoelectrics are also intimately related to multiferroic materials, in which two or all three of (anti)ferroelectricity, (anti)ferromagnetism, and ferroelasticity coexist in the same phase.[2] Inspired by the huge scientific and technological importance of modern magnetic and ferroelectric materials, multiferroic materials have received a lot of attention in the last decades.[3,4] Special device applications for such multiferroic materials have been suggested widely, include multiple state memory elements, electric field controlled ferromagnetic resonance devices and variable transducers with either magnetically-modulated piezoelectricity or electrically-modulated piezomagnetism.[5] Aside from the potential technological applications, the fundamental physics of multiferroic materials is also profuse and fascinating.[6] Experimentally, many efforts have been devoted to seek for new materials with multiferroic properties and find multiferroic properties in already known materials.[7,8] Theoretically, first-principles computational techniques based on density functional theory (DFT) have assisted in designing new multiferroic compounds, and aided in understanding the factors which can promote coupling between electric polarization and magnetization in multiferroic materials.[6,9,10]

The recent revival of interest in multiferroic materials has stimulated the preparation of high-quality Bi-based perovskite and perovskite-related compounds as lead-free ferroelectric and multiferroic materials.[11] The insulating perovskite oxide $BiCoO_3$ has been synthesized by

high-temperature and high-pressure (HP) technique by Belik *et al* in 2006.[12] $BiCoO_3$ is isostructural with the tetragonal ferroelectric compound $PbTiO_3$ (noncentrosymmetric space group P_{4mm}) and has much larger tetragonal distortions (c/a = 1.267, where a and c are the lattice constants) than that of $PbTiO_3$ (c/a = 1.062). The magnetic structure of $BiCoO_3$ was determined by neutron powder diffraction experiments with long-range antiferromagnetic (AFM) order below the Néel temperature (T_N) of 470 K. Giant electric polarization (P_s) of 179 $\mu C/cm^2$ was predicted based on first-principles Berry-phase calculation.[13] First-principles DFT calculations revealed an insulating C-type AFM (C-AFM) ground state in $BiCoO_3$.[12,13,14] $BiCoO_3$ has been suggested to be a promising multiferroic materials exhibiting both ferroelectricity and antiferromagnetism simultaneously. Lately, Sun *et al*. reported that visible light can control the ferroelectricity and magnetoelectric coupling in $BiCoO_3$ nanoribbons for the first time.[15]

The multiferroic material $BiCoO_3$ under hydrostatic pressure has been investigated extensively by DFT theoretical calculations and experimental study. Ravindran *et al.* reported pressure-induced spin state transition from high spin (HS) to low spin (LS) and structural phase transitions from tetragonal ferroelectric (FE) phase to cubic paraelectric (PE) phase with associated insulator to metal transition.[16] Ming *et al*. proposed the pressure-induced structural transition in the HP phase $BiCoO_3$ is isosymmetric accompanied by an insulator to semimetal transition.[17] However, synchrotron X-ray and neutron powder diffraction experiments revealed a polar $PbTiO_3$ type to centrosymmetric $GdFeO_3$ type structural transition above 3 GPa for tetragonal $BiCoO_3$ at room temperature.[18] The first-order transition was accompanied by a drop of electrical resistivity and spin-state change. But a controversial LS spin state in contrast to intermediate spin (IS) state for the HP phase was suggested by structural analysis and X-ray

emission spectra. Based on the experimentally determined crystal structure data of the HP phase, electronic structure calculations demonstrated the semiconducting behavior and LS spin state of the Co^{3+} ion at HP.[19] However, a mixed HS and LS state of the HP phase was suggested recently by electronic structure calculations based on the GGA+U method.[20]

Most of the previous studies focused on the influence of hydrostatic pressure on the properties of the tetragonal $BiCoO_3$. To the best of our knowledge, uniaxial pressure or stress has so far never been applied to the crystal structure, electronic structure, spin state, or polarization properties of $BiCoO_3$. In the present work, we carry out DFT calculations to explore the effects of uniaxial pressure (applied along the *c*-axis) on the properties of the tetragonal $BiCoO_3$. We hope to stimulate further experimental work to test our first-principles prediction of the structural transition, spin crossover, electronic structure variations of this promising multiferroic material.

II. COMPUTATIONAL DETAILS

The *ab initio* calculations performed in this work were done using the CASTEP code,[21] which employs the DFT plane-wave pseudopotential methods. Spin-polarized GGA with PBE form (GGA-PBE) is used to treat the exchange-correlation function.[22] The interactions between the core region and valence electrons are described by Vanderbilt-type ultrasoft pseudopotential.[23] Bi $6s^2$ $6p^3$, Co $3d^7$ $4s^2$ and O $2s^2$ $2p^4$ are treated as valence electrons during calculations. The plane-wave basis set cutoff energy is set to 380 eV and requested *k*-point spacing is fixed to 0.03 $Å^{-1}$ in the irreducible Brillouin zone for all calculations. The convergence thresholds for energy change, maximum force, maximum stress, and maximum displacement between optimization cycles are 5×10^{-6} eV/atom, 0.01 eV/Å, 0.02 GPa and 5×10^{-4} Å.

The initial crystal structural model of tetragonal phase $BiCoO_3$ is built according to the neutron powder diffraction data.[12] The atomic positions are Bi (0, 0, 0), Co (0.5, 0.5, 0.5+Δz), O1 (0.5, 0.5, Δz_1), O2 (0.5, 0, 0.5+Δz_2). The crystallographic primitive cell of tetragonal $BiCoO_3$ consists of one five-atom formula unit, and the C-AFM magnetic cell is a ten-atom $\sqrt{2} \times \sqrt{2} \times 1$ supercell containing two $BiCoO_3$ formulae.[17] According to previous DFT calculations and the experimental observed two-dimensional AFM characteristic, the 10-atom $\sqrt{2} \times \sqrt{2} \times 1$ supercell with C-AFM spin configuration is adopted to simulate the tetragonal $BiCoO_3$ under uniaxial pressure conditions. To calculate the uniaxial pressure along the *c*-axis, we apply a pressure in the [001] direction and conduct elaborate geometry optimization for the atomic internal coordinates and the lattice parameters within the BFGS minimization algorithm.[24] All the structural relaxations are started from a nonsymmetric atomic configuration by switching off the symmetry of crystal structural models (corresponding to the P1 space group) for each value of the applied pressure to implement uniaxial pressure *ab initio* simulations, so that the compound is allowed to find its lowest energy state.

III. RESULTS AND DISCUSSION

Fig. 1 shows the evolution of the structural parameters under uniaxial pressure for the tetragonal $BiCoO_3$. The lattice parameter *a* expands slowly and *c* is compressed gradually along with the uniaxial pressure below 8GPa. The change of *c* axis with pressure is much greater than that of the *a* axis, which exhibiting a remarkable anisotropic compressibility under uniaxial pressure condition. All structural parameters change dramatically from 8 to 9 GPa. The unit cell volume collapse remarkably with a volume decrease of about 9.5% from 8 to 9 GPa. The

discontinuous volume collapse is accompanied with abrupt shrinkages of *a* and *c* axes. The *a* axis shrinks a bit from 3.845 to 3.821 Å, and *c* axis shows a sharp contraction from 4.235 Å to 3.882 Å. The compression behavior of tetragonal $BiCoO_3$ is highly anisotropic with the *c*-axis being the soft direction, which consist with the layered perovskite-type crystal structure. Besides, the tetragonality (the axial ratio *c*/*a*) changes abruptly from about 1.1 to 1.01. The discontinuous transformations of the lattice parameters indicate the phase transition is first order. Though the structural parameters of $BiCoO_3$ displays a prominent variation at 9 GPa, the symmetry has not changed after the phase transition. Therefore, the structural transition at 9 GPa is assigned to a first-order isosymmetric phase transition.

Calculated structural parameters illustrate that a dramatic expansion of the Co-O1 bond length from 1.800 Å to 1.862 Å (expanding by about 3%) and shrinkage of the Co-O2 bond length from 1.991 Å to 1.930 Å (compressing by about 3%). The *a* axis changes from 3.845 Å to 3.821 Å, whereas the *c* axis contracts abruptly from 4.235 Å to 3.882 Å (shrinkage of 8.3%). The atomic internal parameters of the O1 position (Δz_1) change from 0.150 to 0.094 and O2 position (Δz_2) changes from 0.198 to 0.145. The apical O ions (O1) are departing from the Co^{3+} ion in the CoO_5 pyramid and moving towards the face of the lattice, and the equatorial O ions (O2) are moving more close to the face-center of the crystallographic primitive cell. The pressure has caused the coordination environment of the Co^{3+} ion to transform from CoO_5 square-pyramid to the distorted CoO_6 octahedron as shown in Fig. 2.

The spin state of Co^{3+} ions has been a contradictory topic and has lead to intensive debate especially in a CoO_5 pyramidal coordination.[25] It is generally believed that the Co^{3+} ions adopt a LS state in octahedral CoO_6 coordination environments and the IS state in pyramidal CoO_5

coordination environments at low temperature and ambient pressure conditions.[26] In order to ascertain the volume collapse and the discontinuity in the lattice parameters whether relate to the spin state transition as shown under hydrostatic pressure condition,[16,17,18,19,20] we calculated the magnetic moment of tetragonal $BiCoO_3$ under uniaxial pressure. The calculated magnetic moment of Co^{3+} ion is 2.58 μ_B at ambient pressure condition. At the same time, there is residual magnetic moment of 0.50 μ_B for the apical O ions (O1) in the CoO_5 pyramid. The calculated total spin moment of 3.08 μ_B at ambient pressure condition is in good agreement with available experimental value of 3.24 μ_B and previous theoretically calculated results.[12,13,14,16,17,18,19,20] The strong hybridizations of Co-O and Bi-O bonds cause a large reduction of magnetic moment compared with the expected value of 4 μ_B for HS configurations of Co^{3+} ($3d^6$) ions. The experimentally determined HS configuration of the Co^{3+} ($3d^6$) ion at ambient condition has been successfully reproduced.[12]

The calculated magnetic moment of Co^{3+} ion in $BiCoO_3$ as a function of the uniaxial pressure is presented in Fig. 3. We confirm the HS configurations of Co^{3+} ions (S = 2) in the CoO_5 pyramidal coordination below 8 GPa.[12,13,14,16,17,18,19,20] However, the magnetic moment transforms abruptly to 0 at 9 GPa, which indicating that the spin state of the Co^{3+} ions transforms to a nonmagnetic (NM) LS configurations (S = 0) above 8 GPa. Thus the structural transition accompanies with the spin state transformation from HS to LS state of the Co^{3+} ions in tetragonal $BiCoO_3$. Magnetic moment collapse along with volume collapse has taken place upon increasing uniaxial pressure, whereas the crystal structural symmetry has been unchanged under compression.

The class of Cobalt-containing transition metal complexes has attracted considerable interest

in the last decade because of the spin degree of freedom of Co^{3+} ions.[27,28] The 3*d* levels split into nondegenerate b_{2g} ($\boldsymbol{d}_{xy}$), doubly degenerate e_g ($\boldsymbol{d}_{yz}, \boldsymbol{d}_{zx}$), nondegenerate a_{1g} ($\boldsymbol{d}_{z^2}$), and b_{1g} ($\boldsymbol{d}_{x^2-y^2}$) levels in the square-pyramidal crystal field (CF).[16] Three possible spin states of Co^{3+} ions appear as a result of the competition between CF, on-site Coulomb correlation effects and the intra-atomic exchange splitting: the LS state (LS, $b_{2g}^2 e_g^4 a_{1g}^0 b_{1g}^0$, $S = 0$), IS state (IS, $b_{2g}^2 e_g^3 a_{1g}^1 b_{1g}^0$, $S = 1$), and HS state (HS, $b_{2g}^2 e_g^2 a_{1g}^1 b_{1g}^1$, $S = 2$). Though these relevant energy scales are important for the spin state of Co^{3+} ion, only the CF splitting is extraordinary sensitive to pressure or stress. Previous neutron diffraction experiments and first-principle DFT calculations have confirmed definitely the HS states of Co^{3+} ions in tetragonal $BiCoO_3$ at ambient condition.[12,13,14,16,17,18,19,20] It has been established that the competition between the CF splitting and the intra-atomic exchange coupling can induce spin state transition. The intra-atomic exchange coupling favours HS state with a maximum spin multiplicity, whereas the CF splitting favours LS state in which the electrons occupy low-energy orbitals only at the expense of increasing the exchange energy.[29,30] The CF splitting enhances dramatically under pressure. Therefore, system transforms to a LS state when the CF splitting exceeds the Hund's rule exchange energy. In accordingly, the increase of the CF splitting and the transformation of the coordination environment lead to the spin crossover of the Co^{3+} ions from HS to LS states. The 3*d* electrons are pairwise compensated, which leading to the orbital and spin degrees of freedom freeze up in the NM LS state ($S = 0$). The ionic radius of the LS state is smaller than the HS state, which most likely resulting in the volume collapse along with the spin state transition.[31]

Density functional theory became the most popular and useful computational approach in

most branches of chemistry, materials and condensed matter physics.[32,33,34] The popularity of DFT calculations stems from a good balance between reasonable and useful accuracy, speed, lower computational cost, and high computational efficiency.[35] However, it is well known that local spin density approximation (LSDA) and GGA strongly underestimate the electronic band gap, which becomes particularly pathological when an insulator is treated as a metal. Though the insulating ground state of $BiCoO_3$ has been successfully reproduced by first-principles calculations, the calculated band gap values are about 0.6 eV [13], 0.67 eV [17], 0.6 - 0.73 eV [19], 0.9 eV [36], 1.1 eV [37], 0.395 eV [38], and 0.72 eV [39], which are much smaller than the experimental values of 1.7 eV [39]. The difference between the calculated band gaps and experimental results are expected to be due to the underestimation of band gap by the LSDA and GGA methods and also the arrangement of different magnetic configurations in tetragonal $BiCoO_3$.

Used a so-called LSDA+U method, theoretical calculations predict the insulating ground state with a band gap of 2.11 eV (U = 6 eV) in the C-AFM ordering for $BiCoO_3$.[14] DFT calculations with GGA + U exchange-correlation potentials have obtained band gaps of 1.98 eV (U = 6 eV) [20], 1.70 eV (U = 3 eV), and 1.92 eV (U = 6 eV) [36], whereas within the modified Becke–Johnson (mBJ) exchange potential the calculated band gap value increase to 2.49 eV [36]. Sudayama *et al*. performed unrestricted Hartree-Fock calculation on a multiband d-p model with eight Co sites and shown that the C-type AFM structure was the most stable with an overestimated band gap of 3.31 eV.[40] DFT approach produces unsatisfactory band gap for strong electronic correlation system due to the improper treatment of Coulomb correlations. Many practical solutions including DFT + U, hybrid functionals and the self-interaction correction (SIC) schemes

are proposed to solve the band-gap problem, but none has yet become a universal tool of known performance for such systems.[41]

So far, there are seldom hybrid functionals studies dealing with ferroelectric oxides and even less with multiferroic materials.[42,43,44] Hereinafter, we try to calculate the electronic structure within GGA-PBE [22] and B3LYP hybrid functional [45] as implemented in CASTEP code. The hybrid functionals are nonlocal exchange-correlation functionals, and are intended to improve on the description of band gaps in insulators and semiconductors compared with LDA or GGA calculations. However, the calculations with non-local exchange functional in CASTEP code are not compatible with stress calculations and cell optimization, and are only available for norm-conserving pseudopotentials.[46] Therefore, the structures are relaxed within the PBE approximation and are kept fixed for the hybrid functional calculations.[41] In addition, there is an important difference between standard DFT calculations with local exchange-correlation potentials and the nonlocal exchange case. The potential used in the latter scenario depends on the wavefunctions at SCF *k*-points, whereas the potential depends only on electron density in the former case. This difference can make calculations a lot more expensive in terms of memory usage and CPU time. So we use a plane-wave energy cutoff of 610 eV and *k*-point spacing of 0.07 $Å^{-1}$ for the hybrid functional calculations. Bi $5d^{10}\ 6s^2\ 6p^3$, Co $3d^7\ 4s^2$ and O $2s^2\ 2p^4$ are treated as valence electrons during calculations. The interactions between the core region and valence electrons are described by norm-conserving pseudopotentials.[46]

The calculated insulating band gaps for the ground state (C-AFM) tetragonal $BiCoO_3$ are 0.656 eV (GGA-PBE) and 2.478 eV (B3LYP). The hybrid functionals indeed improve the electronic band gap in better agreement with the available experimental data,[39] which consist well

with the calculated band gap value of 2.49 eV within mBJ exchange potential.[36] The exact exchange in hybrid functional corrects the self-interaction of occupied states and results in the occupied valence bands shifting downwards. On the other hand, the unoccupied states are shifted upwards. A larger band gap opens up.[42] Due to the well-known bandwidth broadening, the band gaps reduced to 0.343 eV and 1.133 eV by GGA-PBE and B3LYP calculations under uniaxial compressing of 8 GPa. The band structures of tetragonal $BiCoO_3$ at 0 GPa (ambient pressure condition), 8 GPa (before transition) and 9 GPa (after phase transition) are presented in Fig. 4, where the Fermi level (E_F) is set to 0 eV. The prominent characteristic of the band structures are the spin-*up* and spin-*down* subbands overlap each other, displaying the AFM ordering of the HS state and NM characteristic of the LS state for $BiCoO_3$. The band structure of the LS phase at 9 GPa displays a prominent characteristic of the NM metal by PBE approximation. However, the B3LYP calculated results show an insulating band structure with a band gap of 1.530eV. These controversial results recall the case of $BiCoO_3$ under hydrostatic pressure. First principles DFT calculations reported pressure-induced spin state transition and tetragonal to cubic structural phase transition associated with insulator to metal transition in $BiCoO_3$.[16] Our previous DFT electronic structure calculations with PBE approximation show a volume collapse and spin state transition accompanied by an insulator-to-semimetal transition in $BiCoO_3$ under high pressure.[17] But subsequent experimental results disproved the metallization of $BiCoO_3$ predicted by DFT calculations. $BiCoO_3$ show a semiconducting behavior under high pressure.[18] It is worthwhile to note that in another multiferroic material $PbVO_3$ (isostructural with tetragonal $BiCoO_3$), a tetragonal to cubic structural phase transition occurs from about 2 GPa at room temperature. Though the phase transition accompanied with a significant drop of resistivity by about 5 orders of

magnitude, the cubic HP phase exhibited a semiconducting behavior of resistivity between 2 and 300K up to 11.3 GPa.[47] We propose that the B3LYP calculated result is favorable, and $BiCoO_3$ is a NM insulator under uniaxial pressure. However, we should be aware that spin-state energetics in spin crossover (spin state transition) compounds can depend significantly on the type of functional chosen, in particular on the admixture of exact exchange in hybrid functionals.[34,48] Therefore, complementary heat capacity and resistivity measurements under uniaxial pressure or stress will be invaluable to explore the exact nature of HP phase $BiCoO_3$.

The application of external pressure provides a powerful tool to tune the structural, magnetic and electronic properties of transition metal oxides. Application of uniaxial pressure results in complex phase transitions including structural collapse and spin-state transition, which providing remarkable evidence of strong coupling between the lattice, spin, and charge degrees of freedom in $BiCoO_3$. Due to the coupling interaction of multifold degrees of freedom, tetragonal phase $BiCoO_3$ affords a ground to investigate variously intriguing characteristic and profuse phenomena. Uniaxial pressure tuning of the structure and spin state of $BiCoO_3$ promises to be an intriguing avenue for experimental study. We hope our predictions will further stimulate both experimental and theoretical interests to investigate ferroelectrics and other fundamental physics under uniaxial pressure or stress for multiferroic material.

IV. CONCLUSION

In the present work, we carry out first-principles calculations to simulate the effects of uniaxial pressure on the properties of the tetragonal $BiCoO_3$. The structural parameters, lattice volume, and atomic displacements show abrupt changes near the uniaxial pressure of 9 GPa,

which is related to the dramatic change of magnetic moment and spin state. First-principles study demonstrates that uniaxial pressure inducing the structural transformation and spin state transition of the Co^{3+} ions simultaneously in $BiCoO_3$. PBE calculations predict an insulator-to-metal transition, whereas B3LYP hybrid functional calculated results disprove the metallization of $BiCoO_3$ under uniaxial pressure. Our theoretical computational work calls for further HP experimental investigations as well as other theoretical study to further clarify the nature of the transition and the electronic structure for HP phase $BiCoO_3$.

ACKNOWLEDGMENTS

This work was sponsored by the National Natural Science Foundation of China (Grant Nos. 11104101), Natural Science Foundation of Hubei Province, China (Grant No. 2014CFB439) and the Scientific and Technologic Research Program of Department of Education of Hubei Province, China (Grant No. D20132902).

References

[1] W. Eerenstein, N. D. Mathur, and J. F. Scott, Nature **442**, 759 (2006).

[2] J. F. Scott, NPG Asia Mate. **5**, e72 (2013).

[3] J. Wang, J. B. Neaton, H. Zheng, V. Nagarajan, S. B. Ogale, B. Liu, D. Viehland, V. Vaithyanathan, D. G. Schlom, U. V. Waghmare, N. A. Spaldin, K. M. Rabe, M. Wuttig, and R. Ramesh, Science **299**, 1719 (2003).

[4] M. Fiebig, Th. Lottermoser, D. Fröhlich, A. V. Goltsev, and R. V. Pisarev, Nature **419**, 818 (2002).

[5] Vincent Garcia & Manuel Bibes, Nat. Commun. **5**, 4289 (2014).

[6] N. A. Hill, J. Phys. Chem. B **104,** 6694 (2000).

[7] T. Kimura, T. Goto, H. Shintani, K. Ishizaka, T. Arima, and Y. Tokura, Nature **426**, 55 (2003).

[8] G. Catalan & J. F.Scott, Adv. Mater. **21**, 2463 (2009).

[9] Hong Jian Zhao, Wei Ren, Yurong Yang, Jorge Íñiguez, Xiang Ming Chen and L. Bellaiche, Nat. Commun. **5**, 4021 (2014).

[10] C. Ederer and N. A. Spaldin, Curr. Opin. Solid State Mater. Sci. **9**, 128 (2005).

[11] A. A. Belik, J. Solid State Chem. **195**, 32 (2012).

[12] A. A. Belik, S. Iikubo, K. Kodama, N. Igawa, S. Shamoto, S. Niitaka, M. Azuma, Y. Shimakawa, M. Takano, F. Izumi, and E. Takayama-Muromachi, Chem. Mater. **18**, 798 (2006).

[13] Y. Uratani, T. Shishidou, F. Ishi, and T. Oguchi, Jpn. J. Appl. Phys. **44**, 7130 (2005).

[14] M. Q. Cai, J.C. Liu, G. W. Yang, Y. L. Cao, X. Tan, X. Y. Chen, Y. G. Wang, L. L. Wang, and W. Y. Hu, J. Chem. Phys. **126**, 154708 (2007).

[15] Bai Sun, Hongwei Li, Lujun Wei and Peng Chen, RSC Adv. **4**, 50102 (2014).

[16] P. Ravindran, R. Vidya, O. Eriksson, and H. Fjellvåg, Adv. Mater. **20**, 1353 (2008).

[17] X. Ming, X. Meng, F. Hu, C.Wang, Z. Huang, H. Fan, and G. Chen, J. Phys. Condens. Matter **21**, 295902 (2009).

[18] K. Oka, M. Azuma, W. Chen, H. Yusa, A. A. Belik, E. Takayama-Muromachi, M. Mizumaki, N. Ishimatsu, N. Hiraoka, M. Tsujimoto, M. G. Tucker, J. Attfield, and Y. Shimakawa, J. Am. Chem. Soc. **132**, 9438 (2010).

[19] S. Kanungo and T. Saha-Dasgupta, Phys. Rev. B **83**, 104104 (2011).

[20] Ting Jia, Hua Wu, Guoren Zhang, Xiaoli Zhang, Ying Guo, Zhi Zeng, and Hai-Qing Lin, Phys.

Rev. B **83**, 174433 (2011).

[21] M. D. Segall, P. J. D. Lindan, M. J. Probert, C. J. Pickard, P. J. Hasnip, S. J. Clark, and M. C. Payne, J. Phys.: Condens. Matter **14**, 2717 (2002).

[22] J. P. Perdew, K. Burke, and M. Ernzerhof, Phys. Rev. Lett. **77**, 3865 (1996).

[23] D. Vanderbilt, Phys. Rev. B **41**, R7892 (1990).

[24] B. G. Pfrommer, M. Cote, S. G. Louie, and M. L. Cohen, J. Comput. Phys. **131**, 133 (1997).

[25] Z. Hu, H. Wu, M. W. Haverkort, H. H. Hsieh, H. J. Lin, T. Lorenz, J. Baier, A. Reichl, I. Bonn, C. Felser, A. Tanaka, C. T. Chen, and L. H. Tjeng, Phys. Rev. Lett. **92**, 207402 (2004).

[26] A. A. Taskin, A. N. Lavrov, and Yoichi Ando, Phys. Rev. Lett. **90**, 227201 (2003).

[27] C. N. R. Rao, M. Motin Seikh, Chandrabhas Narayana, Top. Curr. Chem. **234**, 1 (2004).

[28] Yann Garcia, Philipp Gütlich, Top. Curr. Chem. **234**, 49 (2004).

[29] T. Kawakami, Y. Tsujimoto, H. Kageyama, X.-Q. Chen, C.L. Fu, C. Tassel, A. Kitada, S. Suto, K. Hirama, Y. Sekiya, Y. Makino, T. Okada, T. Yagi, N. Hayashi, K. Yoshimura, S. Nasu, R. Podloucky, M. Takano, Nat. Chem. **1**, 371 (2009).

[30] J. Kunes, A. V. Lukoyanov, V. I. Anisimov, R. T. Scalettar, and W. E. Pickett, Nat. Mater. **7**, 198 (2008).

[31] P. G. Radaelli and S. -W. Cheong, Phys. Rev. B **66**, 094408 (2002).

[32] Eugene S. Kryachkoa, Eduardo V. Ludeña, Phys. Rep. **544**, 123–239 (2014).

[33] Kieron Burke, J. Chem. Phys. **136**, 150901 (2012).

[34] M Radoń, Phys. Chem. Chem. Phys. **16**, 14479 (2014).

[35] M. Gruden-Pavlović, S. Stepanović, M. Perić, M. Güellc and M. Swart, Phys. Chem. Chem. Phys. **16**, 14514 (2014).

[36] Aleksandar S. Milošević, Milan V. Lalić, Zoran S. Popović, Filip R. Vukajlović, Opt. Mate. **35**, 1765 (2013).

[37] Y. Okuno, Y. Sakashita, Jpn. J. Appl. Phys. **49**, 09ME08 (2010).

[38] Ulas Koroglu, Suleyman Cabuk, Engin Deligoz, Solid State Sci. **34**, 1 (2014).

[39] J. A. McLeod, Z. V. Pchelkina, L. D. Finkelstein, E. Z. Kurmaev, R. G. Wilks, A. Moewes, I. V. Solovyev, A. A. Belik, E. Takayama-Muromachi, Phys. Rev. B, **81**, 144103 (2010).

[40] T. Sudayama, Y. Wakisaka, T. Mizokawa, H. Wadati, G. A. Sawatzky, D. G. Hawthorn, T. Z. Regier, K. Oka, M. Azuma, Y. Shimakawa, Phys. Rev. B **83**, 235105 (2011).

[41] Manish Jain, James R. Chelikowsky, and Steven G. Louie, Phys. Rev. Lett. **107**, 216806 (2011).

[42] A. Stroppa and S. Picozzi, Phys. Chem. Chem. Phys. **12**, 5405 (2010).

[43] M. Goffinet, P. Hermet, D. I. Bilc, and Ph. Ghosez, Phys. Rev. B **79**, 014403 (2009).

[44] D. I. Bilc, R. Orlando, R. Shaltaf, G.-M. Rignanese, J. Íñiguez, and Ph. Ghosez, Phys. Rev. B **77**, 165107 (2008).

[45] J. P. Perdew, M. Ernzerhof, K. Burke, J. Chem. Phys. **105**, 9982 (1996); C. Adamo, V. Barone, J. Chem. Phys. **110**, 6158 (1999).

[46] D. R. Hamann, M. Schluter, C. Chiang, Phys. Rev. Lett. **43**, 1494 (1979).

[47] Alexei A. Belik, Touru Yamauchi, Hiroaki Ueda, Yutaka Ueda, Hitoshi Yusa, Naohisa Hirao, and Masaki Azuma, J. Phys. Soc. Jpn. **83**, 074711 (2014).

[48] Christopher J. Cramer and Donald G. Truhlar, Phys. Chem. Chem. Phys. **11**, 10757 (2009).

Fig. 1 (Color online) Evolution of the unit cell structural parameters under compression by uniaxial pressure along the *c* axis up to 15 GPa for the tetragonal phase $BiCoO_3$: (a) lattice constants *a* and *c*, (b) volume V, (c) axial ratio *c*/*a*. The solid lines are drawn as a guide to the eye.

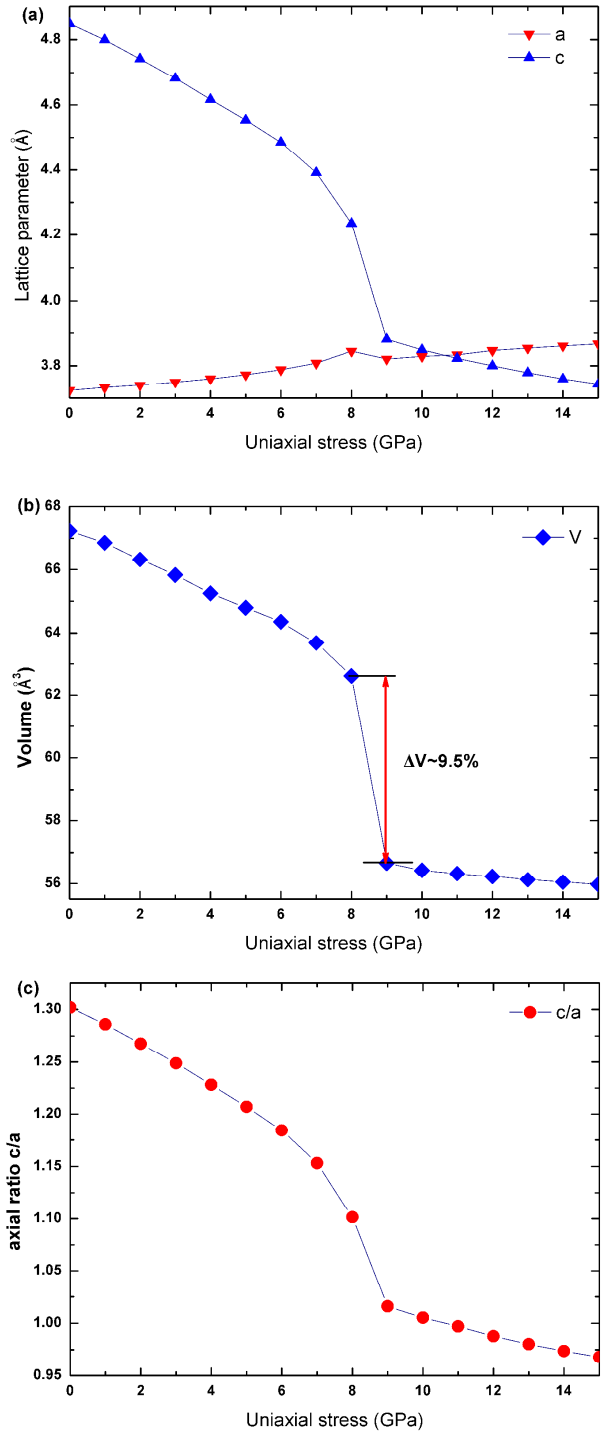

Fig. 2 (Color online) Transformations of the coordination environment of the Co^{3+} ions in tetragonal $BiCoO_3$. The Co-O bong lengths in the local structure are marked, which implying the coordination polyhedron changed from (a) CoO_5 pyramid to (b) distorted CoO_6 octahedron.

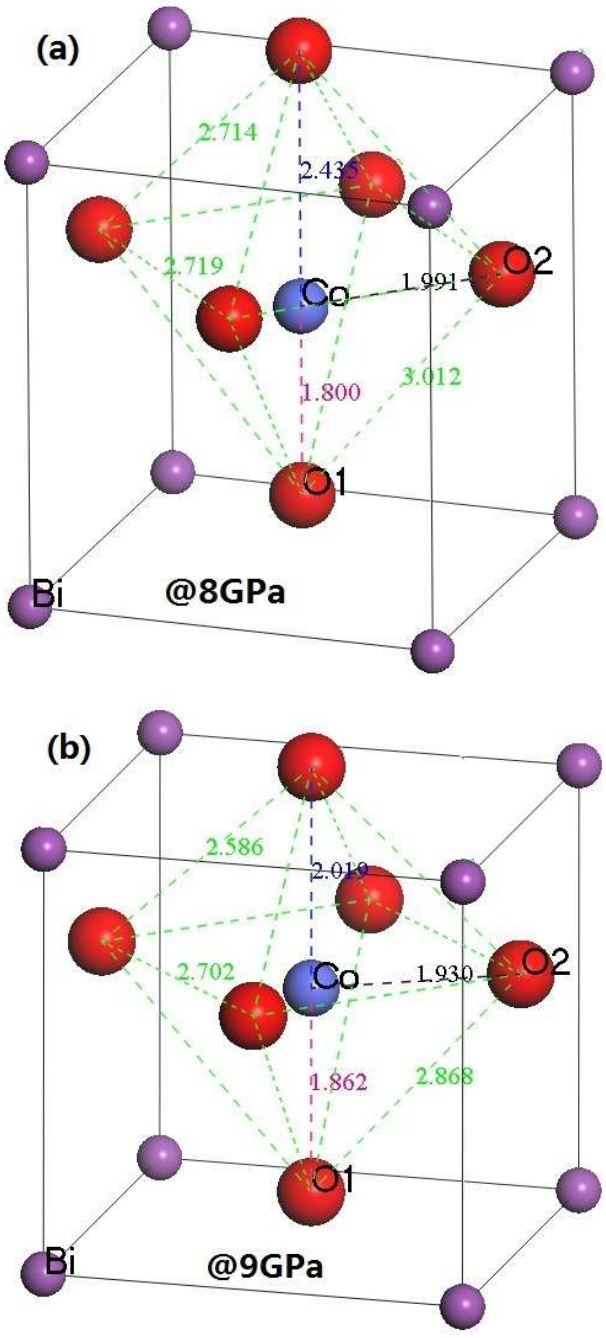

Fig. 3 (Color online) Variation of the calculated magnetic moment (both total and Co^{3+} ions) for tetragonal phase $BiCoO_3$ under uniaxial pressure along the c axis up to 15 GPa. The shadow strip indicates the spin state transition region.

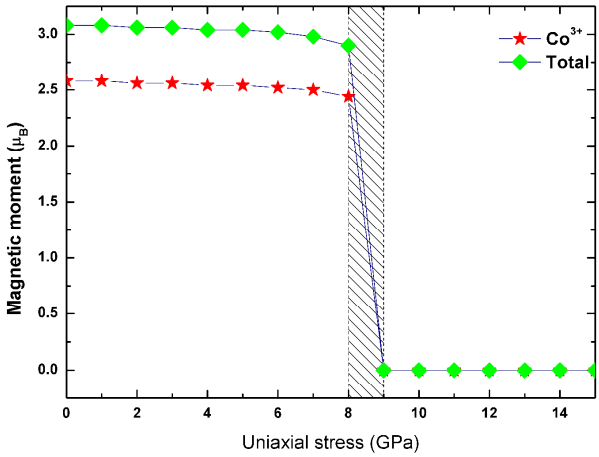

Fig. 4 (Color online) Band structures of the ground state and around phase transitions for tetragonal $BiCoO_3$ calculated by GGA-PBE and B3LYP: (a) and (b) at 0 GPa, (c) and (d) at 8 GPa (before phase transition), (e) and (f) at 9 GPa (after phase transition). Note that the C-AFM spin ordering magnetic cell containing two $BiCoO_3$ formulae before phase transition, whereas the LS phase is nonmagnetic and corresponding to the crystallographic primitive cell (one $BiCoO_3$ formula unit) after phase transition.